Naunyn-Schmiedeberg's Archives of Pharmacology
https://doi.org/10.1007/s00210-025-03994-3

RESEARCH

# Combining computational and experimental approaches: a novel pH-responsive PVA-stabilized MXene nanocarriers/doxorubicin delivery system with enhanced efficacy for targeted lung cancer therapeutics

**Shan Fang[1] · Yuan Li[2] · Wenjuan Wu[3] · Kun He[4] · Nagaraj Patil[5] · Shubham Sharma[6,7,8] · Karthikeyan A.[9] · Dhirendra Nath Thatoi[10] · Azath Mubarakali[11]**

Received: 16 December 2024 / Accepted: 27 February 2025


**Abstract**
While advancements have been made in cancer treatment, achieving effective localized therapy remains a significant challenge. Major obstacles include the inefficiency of drug delivery methods and the side effects linked to traditional chemotherapeutics. In this study, we present an innovative delivery system designed to transport doxorubicin (DOX) directly to the lungs. This system employs PVA-stabilized DOX-loaded MXene, aiming to improve targeted delivery and drug efficacy while minimizing toxicity. Our approach represents a promising advancement in the optimization of cancer therapeutics. Using in silico and computational methods, we evaluated the interactions between PVA, DOX, and MXene. Characterization techniques demonstrated that the synthesized PVA@Mxene/DOX exhibited favorable physicochemical properties. We assessed the anticancer potential of PVA@Mxene/DOX through the MTT assay, in vitro migration assay, and apoptosis assay. The findings revealed that the developed anticancer PVA@Mxene/DOX displayed a layered structure with controlled release kinetics. Notably, it significantly reduced cancer cell growth ($P < 0.05$), induced apoptosis in cancer cells, and inhibited their migration. These results suggest that PVA@Mxene/DOX holds promise as an effective anticancer agent to enhance lung cancer treatment and improve patient care.

**Keywords** Lung cancer treatment · Nursing care · Chemotherapeutic engineering

## Introduction

Lung cancer poses a significant health challenge, particularly for women, where it ranks as the second most prevalent cancer type. Alarmingly, it remains the leading cause of cancer-related deaths among men worldwide, with a disheartening 5-year survival rate of merely 18%. In 2022, lung cancer emerged as the most commonly diagnosed cancer, accounting for nearly 2.5 million new cases, which represents one in every eight cancer diagnoses globally (12.4% of all cancers). It was followed by breast cancer in women (11.6%), colorectal cancer (9.6%), prostate cancer (7.3%), and stomach cancer (4.9%). Additionally, lung cancer was the primary cause of cancer-related fatalities, leading to an estimated 1.8 million deaths (18.7%), with colorectal cancer (9.3%), liver cancer (7.8%), breast cancer (6.9%), and stomach cancer (6.8%) coming next. In terms of prevalence, breast cancer and lung cancer ranked as the most frequently diagnosed cancers among women and men, respectively, for both cases and deaths. (Siegel et al. 2023; Kratzer et al. 2024). This stark statistic highlights the urgent need for innovative research and improved treatment strategies to combat this devastating disease (Siegel et al. 2023). Regretfully, most lung cancers are discovered at an advanced stage. Nevertheless, less than 30% of patients responded to chemotherapy. Even worse, several individuals experienced severe side effects following chemotherapy. The results of those patients have improved with target therapy, particularly with the use of tyrosine kinase inhibitors (TKIs). However, TKIs only help individuals with EGFR mutations, which range from 15 to 50% in Caucasians and 95% of which are adenocarcinomas.

Kun He is solely responsible for entire characterizations and analysis testings.

Extended author information available on the last page of the article

Published online: 29 April 2025

However, there is an urgent need to further investigate useful diagnostic and innovative treatment targets (Zarogoulidis et al. 2013; Yamamoto et al. 2009; Pao and Girard 2011).

The limitations of traditional anti-cancer therapies have prompted researchers to explore the potential of nanotechnology in cancer treatment. Nanomedicine refers to the application of nanotechnology that offers improved effectiveness and enhanced safety (Kawasaki and Player 2005). Nanotechnology-driven therapies provide a range of compelling benefits when compared to standard chemotherapy. They enable precise drug delivery to tumor locations through both passive and active targeting techniques. Additionally, these therapies enhance the solubility and chemical stability of medications, allowing them to remain effective longer in the bloodstream. Another key advantage is the extended circulation time, which improves the likelihood of reaching cancer cells. Moreover, these advanced approaches aim to minimize the toxicity typically associated with traditional cancer treatments and can effectively address drug resistance issues that often undermine treatment success (Biswas et al. 2014; Parhi et al. 2012; Ho et al. 2017). Nanomedicine has gained significant traction in both fundamental research and clinical study due to the rapid advancement of nanotechnology. Targeted nanomedicine has rapidly become a highly promising strategy in the fight against cancer. Breast cancer (BC) stands at the forefront of this research, attracting significant attention due to its diverse characteristics and complicated nature. Researchers are drawn to BC because of issues such as its tendency for drug resistance, high rates of recurrence, and the limited effectiveness of conventional chemotherapy. This intricate landscape makes breast cancer an ideal candidate for innovative treatment approaches using nanotechnology. As an illustration, Abraxane® received approval in 2005 as a conventional therapy for the treatment of metastatic BC. This is a biologically interacting particle of paclitaxel, bound to albumin at the nanoscale. Research findings have shown that this nanoscale albumin-bound paclitaxel has a more effective therapeutic impact and reduced toxicity compared to free paclitaxel when used in the treatment of breast cancer (Miele 2009; Ciruelos and Jackisch 2014). Furthermore, several nanomedicines that have been authorized for clinical use in treating BC also demonstrate significant effectiveness in inhibiting the progression of BC. Moreover, nanomedicine enables the delivery of various therapeutic agents directly to tumor sites using methods like passive targeting, active targeting, and stimuli-responsive targeting. By combining nanomedicine with established treatments such as chemotherapy, radiation, hyperthermia, and immunotherapy, we can create a powerful and promising strategy for effectively battling tumors. This integrated approach holds great potential for improving treatment outcomes and advancing cancer care (Ciruelos and Jackisch 2014).

Today, various types of nanoparticles are making waves in biomedicine and cancer therapy. Among these, gold (Au) and silver (Ag) nanoparticles stand out, along with carbon nanotubes (CNT) and graphene oxide. Additionally, quantum dots (QDs) and MXene materials are gaining attention for their potential applications. These innovative nanomaterials are being harnessed to enhance diagnostic and therapeutic strategies in the fight against cancer. MXenes, which are transition metal carbides, are materials that exist in two dimensions (2D). They possess a wide range of features including a large surface area, high conductivity, and efficient conversion of light into heat. Additionally, they exhibit strong absorption in the near-infrared (NIR) region (Darabdhara et al. 2019; Ahlawat 2020).

MXenes have gained significant attention because of their outstanding electrical conductivity and unique surface properties (Mozafari and Soroush 2021; Khazaei et al. 2017). These materials often demonstrate higher electrical conductivity than graphene, primarily due to their metallic nature resulting from delocalized electrons in their layered structures. The electrical conductivity of MXenes can be fine-tuned by altering their composition and structure; for example, varying the transition metals and surface terminations can modify their electronic properties, making them highly adaptable for applications like energy storage and sensors (Miao et al. 2024; Jiang et al. 2024).

Additionally, the surface of MXenes can be tailored with functional groups (like –OH, –O, or –F) during synthesis, which affects their hydrophilicity (Rizwan et al. n.d.). This characteristic is advantageous for use in catalysis, sensors, and energy storage systems. MXenes typically possess a large surface area, improving their reactivity and performance in applications such as supercapacitors and batteries. Although many MXenes can be chemically reactive, their stability can be boosted through surface functionalization, enhancing their suitability for long-term use (김유진 et al. 2024). In summary, the exceptional combination of high conductivity and adaptable surface properties makes MXenes promising candidates in various fields, including energy storage, electronics, and nanocomposites.

MXenes have diverse applications in various medical domains including drug delivery, biomedicine, cancer therapy, antibacterial treatments, and diagnostics. MXenes are remarkable materials known for their unique structure and electrical properties, making them one of the earliest discovered families of two-dimensional substances. These qualities allow MXenes to be utilized in a variety of applications, showcasing their versatility and importance in advanced material science (Jamalipour Soufi et al. 2022; Maleki et al. 2022). We're focusing on a fascinating class of materials known as chemically etched metal carbonitrides and carbides. These materials can be represented by the general formula Mn + 1XnTx, where "M"

stands for various metal elements like Mn, V, Cr, Hf, Ti, Nb, Zr, Sc, Wd, and others, along with either nitrogen (N) or carbon (C). The variable "n" can take a value of either one or two, while "Tx" indicates additional elements such as oxygen, hydroxyl, or fluorine. These remarkable MXenes are obtained through the etching of MAX phase layers, which include elements like Cd, Ga, Si, As, Al, Ge, In, Ti, and Sn. This process not only reveals their unique properties but also opens up new possibilities for applications in various fields (Paramasivam et al. 2024; Iravani and Varma 2021). The current study hypothesizes that the application of nanotechnology, specifically through targeted nanomedicine, could significantly enhance treatment efficacy and reduce toxicity in lung cancer patients. By harnessing advanced materials like MXenes, which exhibit exceptional electrical conductivity and tunable surface properties, this research aims to explore their potential for targeted drug delivery and therapy, thereby addressing the limitations of conventional treatments and improving patient outcomes in lung cancer care.

## Materials and methods

### Chemical and reagents

Titanium (99.5%, − 325 mesh, aluminum powder (99.5%, − 325 mesh), and graphite (99%, − 325 mesh) were obtained from Alfa Aesar, USA. Poly (vinyl alcohol) (M w = 61,000 g·mol $^{-1}$) was obtained from Sigma-Aldrich.

### Computational method

This study consists of two sections: the first section focuses on DFT-D, while the second section covers MD. Recently, DFT-D has been highlighted as a bridge between traditional empirical concepts and quantum mechanics, enhancing our understanding of electronic properties and the effects of molecules (Ighnih et al. 2023). First principal calculations of all structures (PVA-B) and DOX) were performed with DMol$^3$ program along with PBE-GGA to optimize in Materials Studio version 2017 software (Fig. 1a and b) (Dorairaj

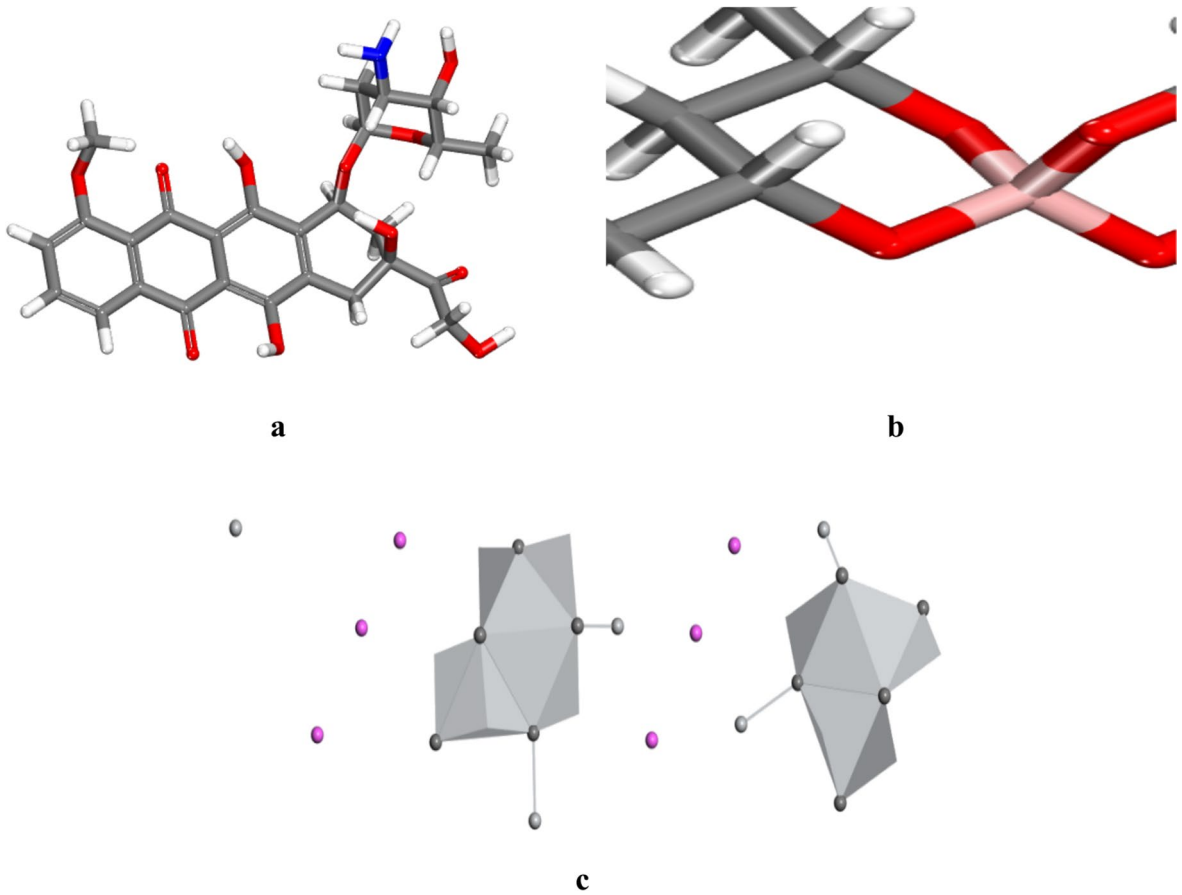


**Fig. 1** **a** The proposed view of DOX structure, **b** PVA-B, and **c** $Ti_3AlC_2$ (104) in Material Studio 2017. Gray in DOX and PVA-B represent carbon atoms and blue in DOX represents nitrogen atoms. Meanwhile, dark and light Gray and $Ti_3AlC_2$ (104) show Ti and C atoms. Pink display Al atom

2023; Balakrishnan et al. 2022). In addition, a Fermi smearing parameter of 0.05 Ha was applied in the DFT-D calculations to enhance convergence by smoothing electron occupancy around the Fermi level, particularly for systems with partially filled electronic states. Additionally, a dipole slab correction was employed to account for the asymmetry in the charge distribution perpendicular to the slab (Gholivand et al. 2023). This parameter smooths the electron occupancy around the Fermi level by introducing a small temperature-like broadening, which helps in stabilizing the self-consistent field (SCF) procedure. In this study, the multipolar expansion approach was employed with the quadrupole moment, enabling a more accurate representation of the charge distribution within the molecular framework.

The monolayer $Ti_3AlC_2$ (104) was then modeled in $a=b=3.07$, $c=18.62$ Å, $\alpha=\beta=90.00$, $\gamma=120.00°$ and volume = 152.17 Å$^3$. An 0.000-Å-thick vacuum space and slab position (1.00) were used in Material Studio 2017 (Fig. 1c). The molecular dynamics simulation (MD) includes an adsorption locator module that is based on the Monte Carlo adsorption locator within an aqueous solution containing six water molecules. Furthermore, the Universal force field is utilized for this calculation (Ganjali Koli et al. 2023).

## Synthesis of MXene

The combination of titanium, aluminum powder, and graphite led to an atomic ratio of Ti:Al:C of 3:1.1:1.8. During the annealing process, equal masses of 5 g were allocated to each powder mixture. The mixtures were then carefully poured into cylindrical alumina crucibles before being placed in a high-temperature furnace manufactured by Carbolite Gero in the UK. The tube underwent purging with argon gas at a flow rate of 50 mL per minute. The furnace temperature was gradually increased to a peak of 1650 °C at a steady rate of 5 °C per minute. Once this maximum temperature was reached, it was maintained for 2 h. Finally, the tube was allowed to cool naturally to the ambient temperature of the surrounding environment.

## Characterization of MXene

To characterize the phase composition of the MAX materials, we utilized X-ray diffraction (XRD) analysis with Ni-filtered Cu–Kα radiation. This analysis was conducted using a Miniflex instrument from Rigaku, operating at 40 kV and 15 mA. Data collection adhered to a step-scan method with a step size of 0.04° and a counting duration of 1 s, covering the 5 to 90° (2θ) range. The morphologies of MXene flakes were examined using scanning electron microscope (SEM). For visualization, we prepared a dilute solution of Ti3C2Tx (less than 0.05 mg/mL) and applied it to a porous alumina membrane (Anodisc, 0.1 µm pore size, from Whatman) via drop casting. The electrical conductivity of the MXene films was measured using a four-point probe apparatus (ResTest v1, Jandel Engineering Ltd., Bedfordshire, U.K.), with probes spaced 1 mm apart.

The FTIR spectroscopy was conducted using JASCO V-530 spectrophotometer (JASCO Co., Tokyo, Japan) using KBr pellets in the frequency range 4000–400 cm$^{-1}$. The dynamic light scattering (DLS, Zetasizer NANO-S90, Malvern, UK) was used to measure the hydrodynamic diameter. A zeta potential analyzer (Zetasizer Nano-ZS, Malvern, UK) was used to measure the zeta potential.

## Conjugation of DOX with MXene

The conjugation of MXenes with DOX was carried out using the dialysis method (Aryal et al. 2009). Briefly, MXenes (1 mg/mL) were dispersed in milli-Q water and mixed with DOX solution (0.2 mg in water pre-treated with 25 µl of 0.15 mM trimethylamine. The required energies for the conjugation were induced via the sonication (five times for 2 min). Then, the mixture was dialyzed overnight, filtered with a 0.8-µm syringe filter, and lyophilized.

## DOX release kinetics study

The release profile of DOX from the nanoformulation was assessed using the dialysis membrane technique (Ramalingam et al. 2018). To prepare a dispersion of synthesized nanoparticles (NP) at a concentration of 100 µg/ml, we placed the nanoparticles in a dialysis membrane with a molecular weight cutoff of 10 kDa. This setup was dialyzed against 25 ml of 1 × phosphate-buffered saline at pH 7.4 and acetate buffer at pH 5. The release buffers were stirred gently at 37 °C and were periodically replaced during the dialysis process. To maintain optimal sink conditions, we substituted 2 mL samples from the measuring aliquot with fresh buffer solutions at the designated pH. The concentration of doxorubicin (DOX) in the samples was measured using a UV spectrophotometer set to 490 nm.

## Cytotoxic activity

To assess the cytotoxic effects of nanoformulation on A549, we performed an MTT assay. Initially, $5 \times 10^4$ cells per well were plated in a 96-well format and allowed to incubate at 37 °C in a controlled environment of 5% $CO_2$ and 95% relative humidity for 24 h. Afterward, the cells were treated with different concentrations of the nanoformulation and incubated for an additional 24 h. Following the treatment, we added 25 µL of MTT solution (5 mg/ml) to each well and allowed it to incubate for 4 h. Next, dimethyl sulfoxide (DMSO) was added to dissolve the formed formazan crystals, and the media was replaced with fresh cell culture medium. Control

wells remained untreated, and we measured the absorbance at 570 nm using an ELISA plate reader to assess cytotoxicity.

### Double AO/EB staining apoptotic cells

We employed dual AO/EB fluorescent staining to identify alterations in cell membranes linked to apoptosis after treatment with the nanoformulation (Geethakumari et al. 2022). Cells were plated at a density of $1 \times 10^5$ cells per well on glass coverslips in a 6-well culture plate and incubated for 24 h at 37 °C in a 5% $CO_2$ atmosphere. After this incubation period, the cells were treated with the IC50 concentration of the nanoformulation for an additional 24 h. Following the treatment, the cells were rinsed twice with PBS and stained with AO/EB at a concentration of 50 µg/ml for 5 min. The stained cells were then observed using fluorescent microscopy, utilizing an excitation filter set to 480/30 nm.

### Migration/invasion assay

Cell migration is an essential process for all living cells, playing a key role in various biological events, from normal development and immune responses to pathological conditions like cancer metastasis and inflammation. Gaining insights into how cells move is important across several biomedical disciplines, including cancer biology, immunology, vascular biology, cell biology, and developmental biology. In this study, after incubating the cells for 24 h, we treated them with a combination of free cell culture media and a nanoformulation. We then harvested the cells through trypsinization in preparation for migration and invasion assays. For the migration study, we placed 100,000 cells in the upper chamber of a Transwell plate, which contained 200 µL of serum-free media. The lower chamber was filled with 700 µL of culture media supplemented with 20% fetal bovine serum (FBS). Following a 15-h incubation at 37 °C, we fixed the filters in methanol for 15 min and stained them with crystal violet for another 15 min. Non-migrated cells on the upper side of the membrane were gently removed with a cotton swab. We analyzed nine random microscopic fields at a magnification of × 200 to determine the average cell migration. For the invasion assay, we pre-coated the upper chamber membrane with 100 µL of Matrigel (BD Biosciences, Bedford, MA) at a concentration of 2.5 mg/mL.

### Statistical analysis

For the statistical analysis, we used SPSS version 18.0. The results are displayed as mean values with standard deviation (SD). To compare the two groups, we applied the Student's *t*-test. For comparisons among multiple groups, we conducted a one-way ANOVA, followed by either the LSD or Dunnett's test. A *p*-value of less than 0.05 was regarded as statistically significant, indicating substantial differences in the data.

## Results

### Simulation results

#### Optimization of structures

In this work, the optimization of DOX and PVA-B structures was studied using first-principles calculations based on DFT-D (Ighnih et al. 2023). Geometry-optimized structures are depicted in Fig. 2a and b. Total DFT-D energy was calculated at − 1927.658 and − 718.560 Ha, respectively.

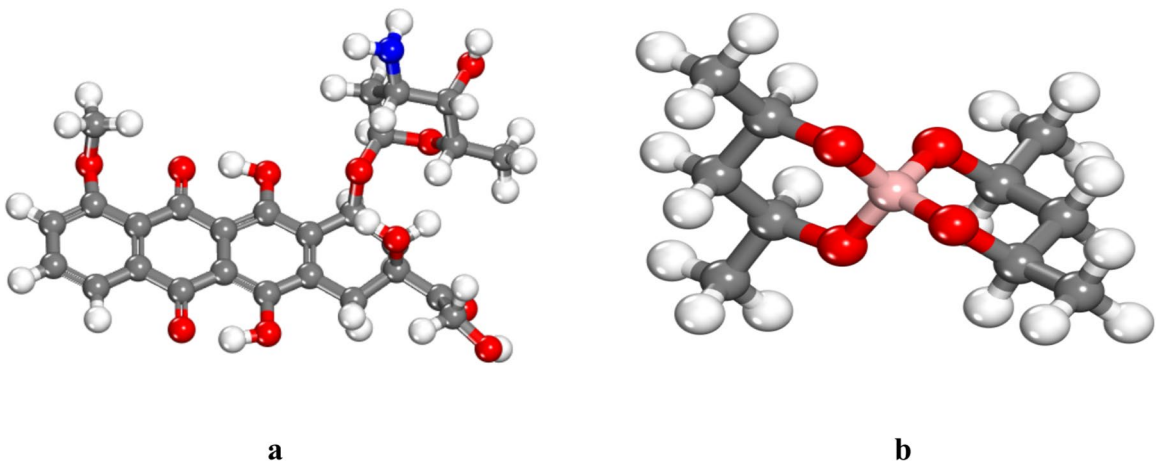

**Fig. 2** The optimized structure of **a** DOX and **b** PVA-B obtained DFT-D method based on DFT-D

### HOMO and LUMO configuration

The concept of HOMO and LUMO orbitals provides valuable insight into potential adsorption sites for interaction (Dorairaj et al. 2023). Figure 3 illustrates the molecular orbitals of the synthesized inhibitors. Specifically, in Fig. 3a, the HOMO and LUMO orbitals of doxorubicin (DOX) are predominantly spread across the anthracene structure and the oxygen atoms connected to it. In contrast, Fig. 3b reveals that the HOMOs of PVA-B are primarily localized on the oxygen atoms, while the LUMO orbitals are largely concentrated on the carbon atoms. These distributions play a crucial role in understanding the interaction characteristics of these compounds. The HOMO and LUMO energies of DOX were calculated to be − 6.596 eV and − 1.236 eV, respectively. For PVA-B, the HOMO and LUMO energies were calculated to be − 6.248 eV and 1.371 eV, respectively. These energy values provide insight into the electronic properties of DOX and PVA-B, and the energy gap (ΔE) between the HOMO and LUMO is an important factor in determining their reactivity, stability, and potential interactions in drug delivery systems. The HOMO and LUMO energies of DOX and PVA-B provide insights into their electronic properties, which affect their behavior in drug delivery systems. DOX has a larger energy gap (5.360 eV), indicating lower reactivity and greater stability, which is beneficial for storage and handling. However, it may require more energy to undergo electronic transitions, limiting its reactivity in biological environments. PVA-B, with a smaller energy gap (7.619 eV), may have better stability but could interact less efficiently with other molecules. The combination of DOX and PVA-B offers a balance between stability and reactivity, allowing for optimized drug delivery, binding efficiency, and therapeutic effects.

### MD simulation

In order to investigate the interaction mechanism and the adsorption behavior between the two DOX molecules and $Ti_3AlC_2$ (104), molecular dynamics (MD) simulation was implemented. Side views of the most stable adsorption configuration of DOX over the $Ti_3AlC_2$ (104) area in the presence of 6 water molecules are presented in Fig. 4a and b. The adsorption energy value ($E_{ads}$) of DOX over $Ti_3AlC_2$ (104) was measured at $-2.140 \times 10^{-3}$ kJ/mol. Negative adsorption energy demonstrated that the adsorption process

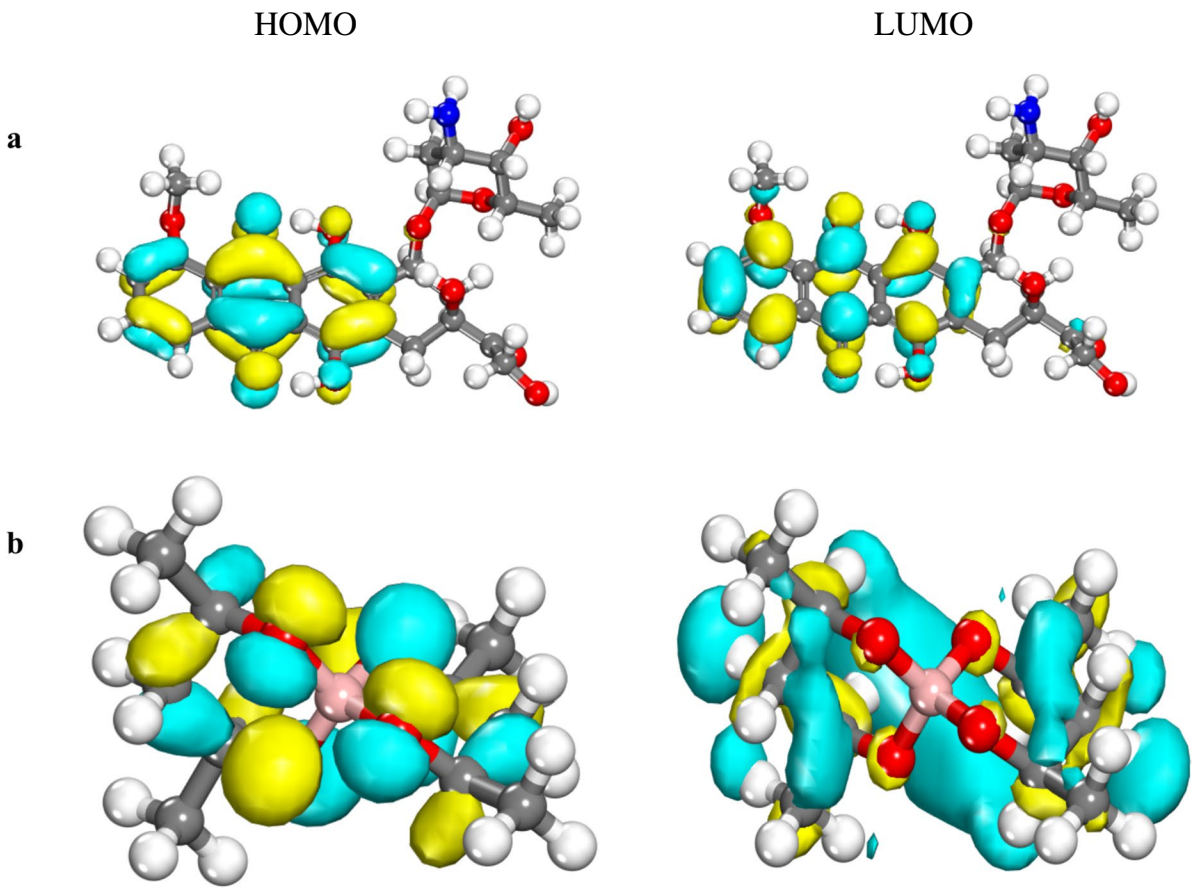


**Fig. 3** Frontier molecular orbitals of **a** DOX and **b** PVA-B were obtained DFT-D method

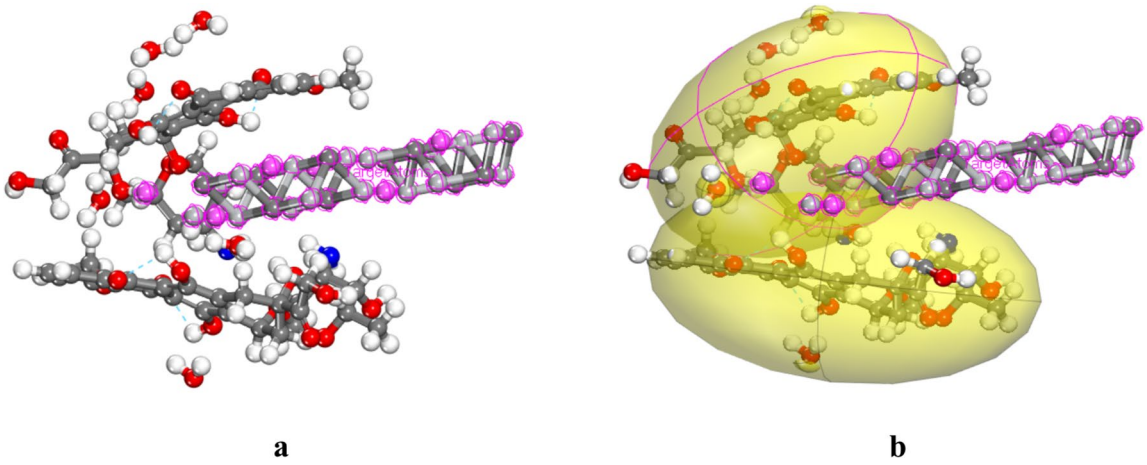


**Fig. 4** The most stable low-energy configuration of DOX over $Ti_3AlC_2$ (104) resulted from Monte Carlo adsorption locator

was exothermic and this system is thermodynamically stable with the most energetically favorable sites. As seen in this figure, the adsorption was physisorption (Haounati et al. 2023a). The results indicated that the adsorption of 2 DOX molecules on the $Ti_3AlC_2$ (104) surface mainly by forming Van der Waals bonds and electrostatic interactions. It is possible to see that DOX adsorbed on the $Ti_3AlC_2$ area via -OH and -$NH_2$ heteroatoms (nitrogen and oxygen).

In the continuous study, the configuration of four PVA-B molecules on the DOX/ $Ti_3AlC_2$ (104) surface was performed by using Monte Carlo adsorption locator in Material Studio 2017. MD calculations showed the DOX/ $Ti_3AlC_2$ (104) decorated PVA-B was stable due to negative (− 79.695 kJ/mol), suggesting preferential adsorption on DOX/ $Ti_3AlC_2$ (104). A negative adsorption energy signifies a favorable interaction between the drug and the delivery system, indicating strong adhesion of the drug to the carrier. The more negative the energy value, the stronger this binding becomes. Such strong adhesion helps prevent the premature release of the drug before it reaches its intended target. Additionally, high adsorption energy suggests that the drug will likely remain attached to the carrier during storage and transport, which enhances the overall stability of the drug delivery formulation a key factor in maintaining drug efficacy over time. The adsorption energy also impacts the rate at which the drug is released from the delivery system. Drugs with strong adsorption may be released more slowly, allowing for a sustained release profile, which is particularly beneficial for treatments that require long-term use or localized therapy. Moreover, the efficiency of drug delivery is closely related to how well the drug interacts with biological tissues after its release. Striking the right balance in adsorption energy can help optimize drug release rates and improve bioavailability, ensuring that the drug reaches an effective concentration at the target site within the body. Understanding adsorption energy is essential for designing formulations that achieve desired release profiles, thereby optimizing drug delivery systems for specific therapeutic applications. By fine-tuning these energy values, researchers can improve treatment outcomes and enhance the overall reliability of drug delivery systems. As depicted in Fig. 5a and b, the results of loaded structures displayed that adsorption of PVA-B on the DOX/ $Ti_3AlC_2$ (104) system led to the structural distortion of DOX and also significantly changed further wrinkle structure. Following $E_{ads}$ negative value confirmed spontaneous adsorption, resulting in strong adsorption and the stability of adsorbate (PVA-B) on the DOX/ $Ti_3AlC_2$ (104) area (Haounati et al. 2023b).

## Mxene properties

The morphology of the synthesized MXene was analyzed using SEM imaging. Figure 6 clearly shows the layered structure of the synthesized MXene. Scanning Electron Microscopy (SEM) is a powerful technique that magnifies extremely small features or structures that are typically invisible to the naked eye. Unlike optical light microscopes that use light for imaging, SEM utilizes electron beams. Because electrons have a shorter wavelength, they enable a more detailed analysis of materials. SEM imaging is commonly employed to assess the results of nanomaterial synthesis processes, providing crucial morphological information for materials scientists studying the target material.

Using the Zeta seizer, the zeta potential of the synthesized nonocomplex was measured, and the results (Fig. 7A) showed that the synthesized nonocomplex has a zeta potential of around − 29.8 mV. It has been shown that a high zeta potential value enhanced the long-term stability of the colloidal systems. The observed high negative zeta potential can be attributed to the OH groups on the surface of

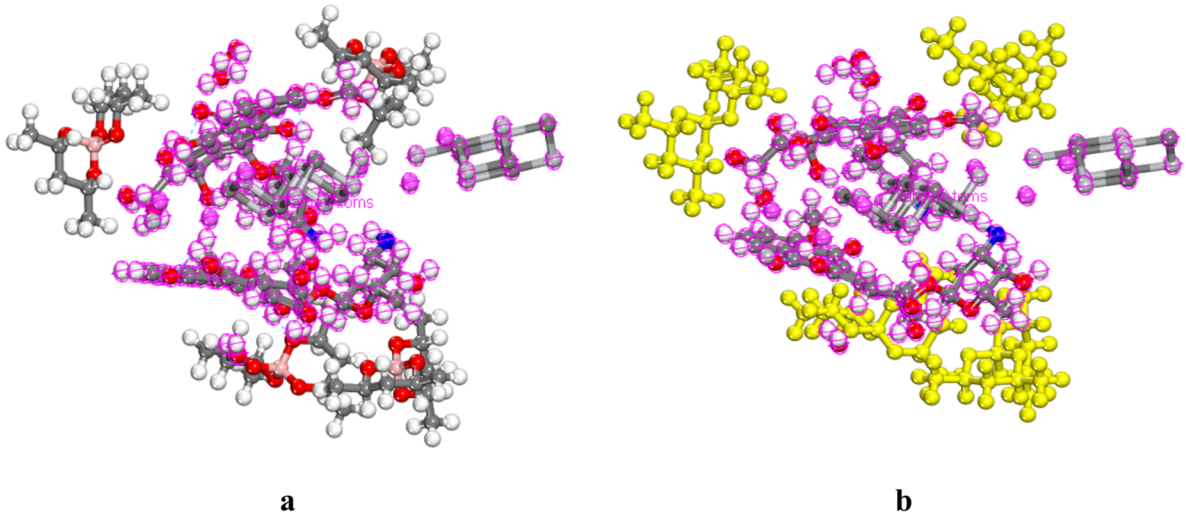


**Fig. 5** The adsorption configuration of PVA-B adsorbed on DOX/ $Ti_3AlC_2$ (104) resulted from Monte Carlo adsorption locator

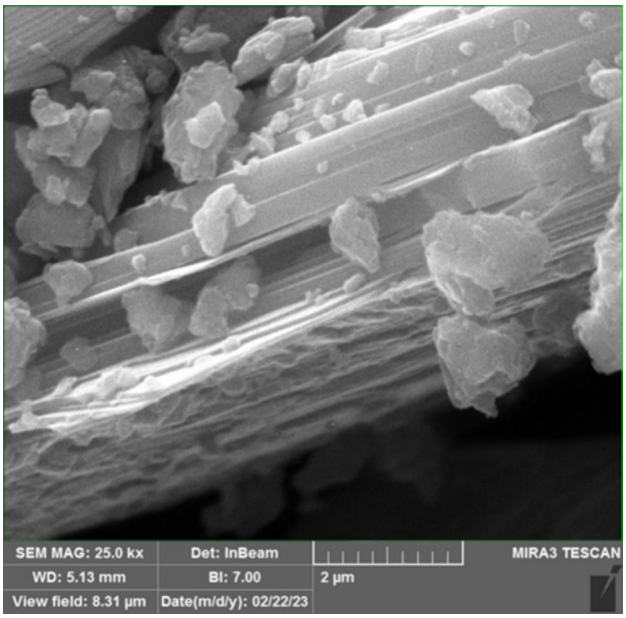


**Fig. 6** SEM image of the synthesized MXenes

nonocomplex (Sun et al. 2021; Urso et al. 2022). The DLS technique was conducted to measure the hydrodynamic size of the nonocomplex, and the results are presented in Fig. 7B. The crystallinity of the nonocomplex was evaluated using the XRD analysis, and the results are presented in Fig. 7C. The results showed that the nonocomplex exhibited a sharp peak around 40° which correspond to (104) crystal plane that is in accordance with $Ti_3AlC_2$ MAX phase (Rasid et al. 2017; Lele et al. 2023). The FTIR spectroscopy was conducted to assess the surface functional groups of the nanocomplex and the results are presented in Fig. 7D. The peaks located at around 3430 $cm^{-1}$ and 1622 $cm^{-1}$ can be related to the vibration peaks of the OH groups. The peak located at around 540 $cm^{-1}$ can be attributed to the stretching vibration peak of Ti–O-Ti. Moreover, the peaks at 3427 $cm^{-1}$, 1620 $cm^{-1}$, and 1090 $cm^{-1}$ in DOX@MXenes nanosheets confirm the DOX conjugation on the surface of MXene. These findings revealed that DOX@MXenes nanocomplexes were successfully fabricated by facile condensation.

The elemental analysis of the synthesized MXene was performed using the EDX technique. EDX, or energy-dispersive X-ray spectroscopy, is a valuable method for analyzing and characterizing samples to better understand their properties. Analyzing elemental composition is essential for gaining insights into unknown substances, the makeup of coatings, materials in small components, quickly identifying alloys, evaluating corrosion, and mapping the distribution of various phases. EDS technology provides both qualitative and quantitative analyses, along with elemental maps, which are useful for studying microstructure in materials research. Although EDS is not typically preferred for examining the chemical composition of specimens due to the limited impact of atomic bonding influenced by local chemical environments, it remains highly effective for determining the elemental distribution within a sample. One of the advantages of EDS is its minimal setup requirements and versatility, as it can be applied to samples of various thicknesses, ranging from semi-thin to bulk, without specific limitations. The results (Fig. 8) indicated that the synthesized MXene comprises Ti, Al, and C.

## In vitro release of drug

We evaluated the in vitro drug release from the nanoformulation at two different pH levels (pH 5 and pH 7.4), as shown in Fig. 9. The results demonstrated that the drug release from

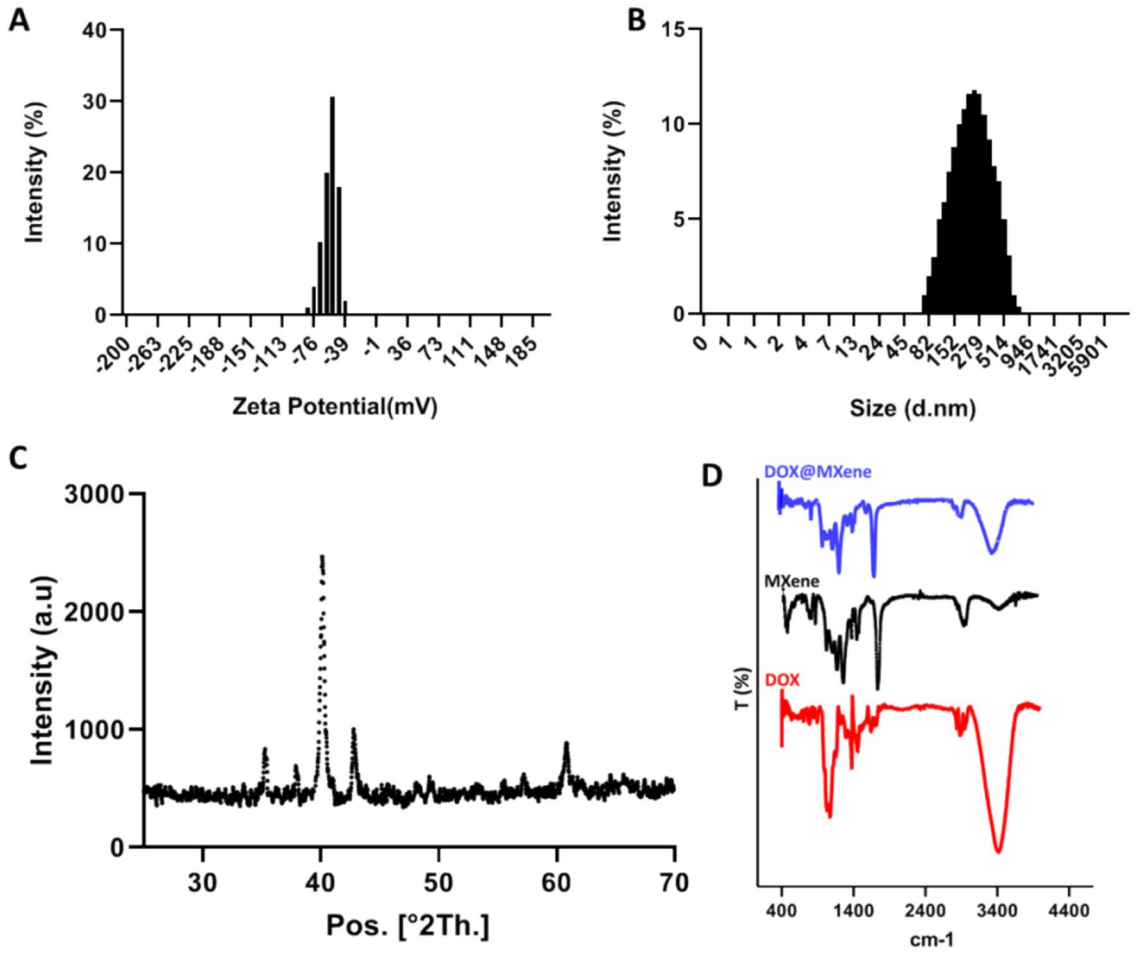


**Fig. 7** Physicochemical properties of the nanostructure. **A** Zetal potential, **B** Hydrodynamic size, **C** XRD pattern, and **D** FTIR spectra

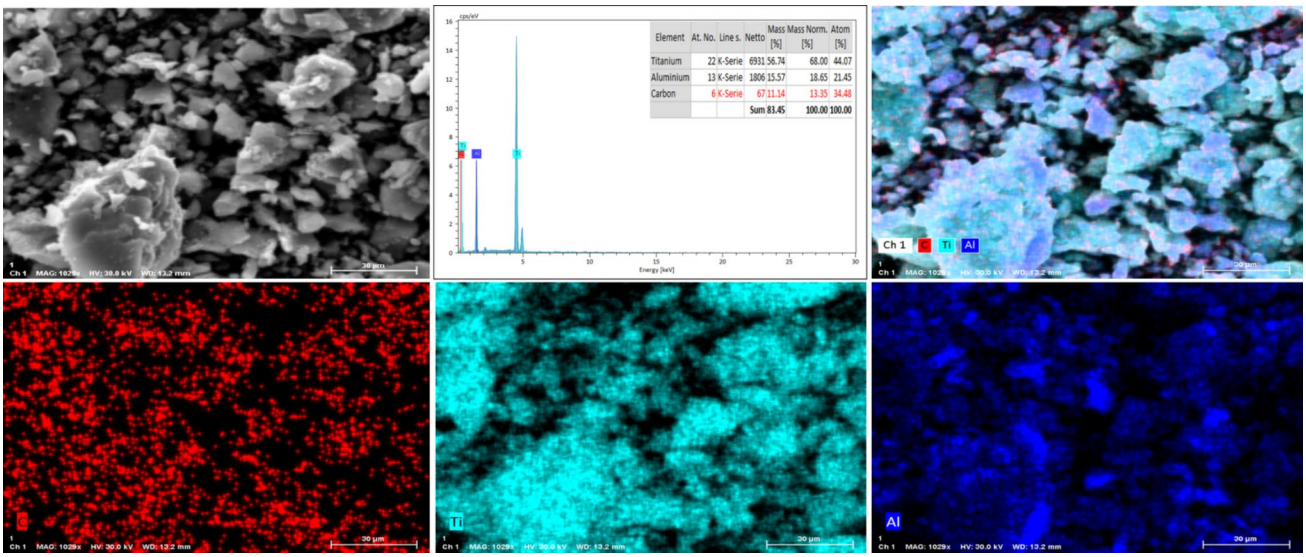


**Fig. 8** EDX results of the synthesized MXene

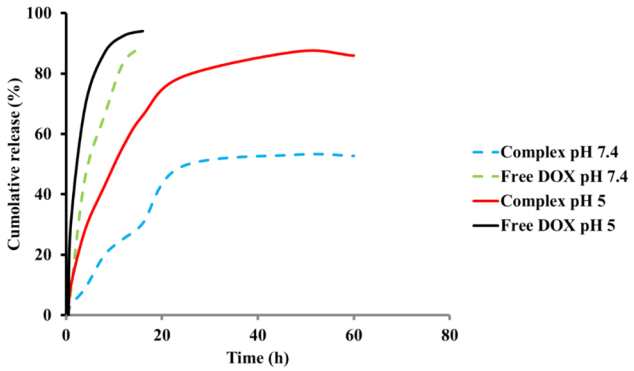


**Fig. 9** In vitro drug release of Free DOX and Conjugated DOX at 37 °C in different pH (pH 5 and pH 7.4)

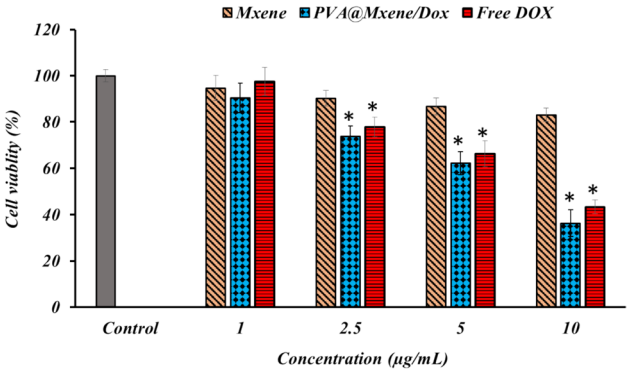


**Fig. 10** Cancer cell's cytotoxic activity of different concentrations (0–10 µg/ml) of the nanoformulation and free DOX. Measured by the MTT assay. (*) $p < 0.05$ compared with control. *n*: 5

the nanoformulation changed over time and was affected by the pH conditions. During the initial phases, both pH levels exhibited a burst release within the first 10 h, followed by a sustained release for the remainder of the 60-h study. At neutral pH (7.4), the maximum release observed was 52.7 ± 5.7% at 60 h, whereas at the acidic pH (5), the release reached 87.2 ± 8.6%. This indicates that a decrease in pH accelerated the drug release. The free DOX reached the highest percentage of release less than 10 h, indicating fast leakage and clearance. The sustained release using the nanocomplex is in agreement with previous reports. Ruan et al. showed that (Ruan et al. 2015) DOX release from the Dox-AuNPs complex was faster at acidic pH. They proposed that the acidic pH accelerated the hydrolysis of the bonds (hydrazone bonds) between DOX and AuNPs. In another study, Ramalingam et al. (2018) conjugated DOX to PVP-stabilized AuNPs and observed a pH-dependent release.

## Cytotoxic activity

One widely used method in toxicological research to evaluate how a drug influences cellular functions like apoptosis, proliferation, and other metabolic processes is cytotoxicity testing. We assessed the anticancer effectiveness of the nanoformulation at various concentrations (0–10 µg/ml) using the MTT assay, with the results shown in Fig. 10. Interestingly, the pure MXene exhibited only minor cytotoxic effects, suggesting it could serve as a safe drug delivery vehicle. This indicates that MXene may have significant potential for future therapeutic applications while posing minimal risk to healthy cells. The lowest cell viability observed when cells were incubated with pure MXene at 10 µg/mL was 83.0 ± 2.9%. In contrast, the synthesized nanoformulation caused a significant, dose-dependent toxicity to the cells, with the lowest cell viability at 10 µg/mL dropping to 36.2 ± 5.7%. Moreover, free DOX induced a dose-dependent cytotoxicity, while its toxicity was slightly lower than the nanoformulation. The observed toxicity for free DOX was not statistically different than the nanoformulation.

The enhanced cancer cell toxicity via MXene conjugation revealed the beneficial role of the conjugation process. The low toxicity of pure MXene is primarily attributed to their composition and structure, which can minimize harmful interactions with biological systems. As a result, they are often considered suitable carriers for therapeutics because they can facilitate the targeted delivery of drugs with a lower risk of adverse effects. However, it is important to note that while MXenes exhibit low toxicity in many studies, the potential for toxicity in long-term exposure isn't fully understood. Factors such as the specific type of MXene, its functionalization, dosage, route of administration, and the biological environment can all influence its safety profile. Long-term studies are essential to evaluate these aspects comprehensively and to ensure that there are no cumulative negative effects or unforeseen reactions over extended periods. In summary, while MXenes show promise as safe carriers due to their low toxicity, ongoing research and long-term studies are necessary to better understand their effects and ensure safety in medical applications.

MXenes, a class of two-dimensional materials, have been studied for their potential applications in various fields, including biomedicine and cancer therapy. The mechanism of higher cytotoxicity and cellular uptake of MXenes in lung cancer involves several factors:

Surface chemistry: The surface chemistry of MXenes can be modified through functionalization. The presence of various functional groups (e.g., –OH, –O, –F) can enhance their interactions with cancer cells, leading to increased cellular uptake. These functional groups can facilitate endocytosis, allowing MXenes to enter cells more efficiently.

High electrical conductivity: MXenes possess high electrical conductivity, which can influence their interaction with cancer cells. When exposed to an electric field, MXenes may generate reactive oxygen species (ROS) that lead to increased oxidative stress in cancer cells, contributing to their cytotoxic effects.

Size and shape The unique size and shape of MXenes (often nanoscale) can also enhance their ability to penetrate biological barriers and be taken up by cancer cells. Smaller nanoparticles can easily pass through cellular membranes and be internalized, resulting in improved cytotoxicity.

Targeting mechanisms: MXenes can be engineered to target specific markers on lung cancer cells. By attaching ligands or antibodies that bind to these markers, the selectivity and accumulation of MXenes in cancerous tissues can be enhanced, leading to increased cytotoxicity while sparing healthy cells.

Stability and biocompatibility: The stability of MXenes in biological environments is crucial for their effective use in cancer therapy. Biocompatible MXenes can achieve prolonged circulation times in the bloodstream, allowing for better accumulation in tumor tissues through the enhanced permeability and retention (EPR) effect.

Induction of apoptosis: Studies have shown that MXenes can induce apoptosis (programmed cell death) in cancer cells via various pathways, including mitochondrial dysfunction and activation of caspases. This contributes to their cytotoxicity against lung cancer cells.

Synergistic effects with therapeutics: MXenes can potentially enhance the effects of existing chemotherapy drugs or radiotherapy. By combining MXenes with traditional therapies, the overall therapeutic efficacy can be increased, resulting in higher cytotoxicity against lung cancer cells. In summary, the higher cytotoxicity and cellular uptake of MXenes in lung cancer can be attributed to their unique properties, including surface chemistry, electrical conductivity, size, targeting mechanisms, stability, and potential for inducing apoptosis. These attributes make MXenes promising candidates for targeted cancer therapies in the future.

## Apoptosis of cancer cells

We applied the acridine orange/ethidium bromide double-staining and the results are presented in Fig. 11. AO is a dye that specifically stains the nuclei of both living and deceased cells in a green color, whereas EB exclusively stains the nuclei of cells with compromised membrane integrity in a red color. Consequently, early apoptotic cells exhibit a crimson hue, whereas healthy cells display a green color. Red hues represent cells in the late apoptotic stage. The results show that the DOX@MXenes displayed distinct yellowish-red and red staining patterns, while the green staining of the nuclei noticeably diminished. This finding indicates that cellular damage and apoptosis are taking place. Apoptosis, the body's inherent process of programmed cell death, can be seen across various tissues. It is marked by distinct physical changes and notable fragmentation of DNA. In order to evaluate the cell death mechanism induced by NPs, we analyzed the changes in cell structure that are often linked with apoptosis using the AO/EB staining technique. The penetration

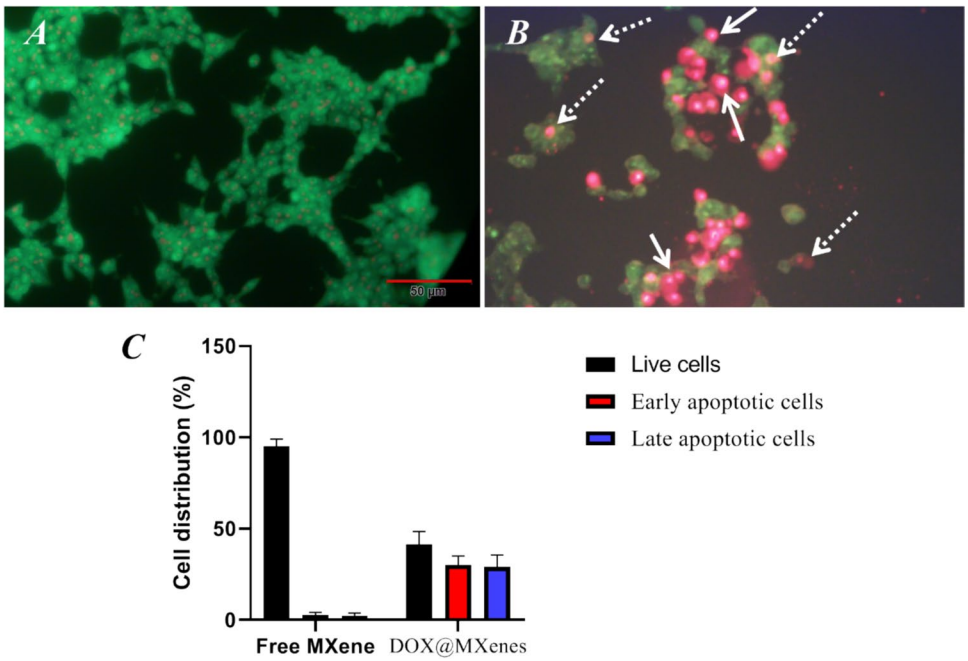


**Fig. 11** Cells were subjected to acridine orange/ethidium bromide double-staining while incubated with two different substances: **A** free MXene, **B** DOX@MXenes, and **C** Quantified results. During this analysis, early apoptotic cells were highlighted with white arrows, while dashed arrows pointed to late apoptotic cells

of acridine orange into the cellular membranes of living cells resulted in their fluorescence in green color. Nevertheless, the treated cells experienced apoptosis, resulting in nuclear shrinkage and emitting an orange fluorescence. Oxidative stress is a critical determinant that leads to cellular damage and significantly contributes to the development of cancer.

### Cell invasion assay

For cells to function effectively, they need to navigate and position themselves optimally within their environment. Tumor cells showcase this ability by migrating from the original tumor site through the lymphatic and circulatory systems, breaching basement membranes and endothelial layers, and ultimately establishing colonies in distant organs. This complex process, known as invasion and metastasis, hinges on key actions like cell migration, invasion, and adhesion, making their study crucial in our fight against cancer. The spread of cancer cells to peripheral organs contributes significantly to cancer-related morbidity and mortality. In our investigation, we utilized a transwell cell migration and invasion assay to assess the anti-metastatic properties of a novel nanoformulation. The results (Fig. 12) demonstrate that the anti-metastatic effectiveness of DOX@MXenes was significantly superior to that of pure MXenes.

## Discussions

The results of this study demonstrate significant advances in the development of a doxorubicin (DOX) conjugated MXene platform for enhanced lung cancer treatment, drawing on a multifaceted approach that includes computational modeling, drug release testing, cytotoxicity assays, and apoptosis evaluation.

### Geometrical and energetic characterization

Starting with our computational results, first-principles calculations based on DFT-D provided valuable insights into the optimized structures of DOX and PVA-B, highlighting their geometric stability (shown in Fig. 2a and b). The calculated total DFT-D energies of − 1927.658 Ha for DOX and − 718.560 Ha for PVA-B underscore the favorable energetic profiles of these compounds. Understanding these geometries is crucial for predicting their behavior in a biological setting. The analysis of the highest occupied molecular orbital (HOMO) and lowest unoccupied molecular orbital (LUMO) configurations (depicted in Fig. 3) reveals the potential adsorption sites for these molecules. The electronic distribution in DOX seems to center around its anthracene structure, indicating sites for potential interaction with target surfaces. In contrast, PVA-B displays localization on its oxygen atoms, which suggests electrostatic interactions may play a significant role in its reactivity and binding properties (Oliveira and Guidelli 2021; Yao et al. 2022).

### Molecular dynamics simulations

The molecular dynamics (MD) simulations further elucidated the interaction dynamics between DOX molecules and the $Ti_3AlC_2$ (104) surface. The measured adsorption energy of $-2.140 \times 10\text{^}-3$ kJ/mol signifies an exothermic interaction, affirming that the adsorption process is energetically favorable due to physisorption driven primarily by Van der Waals forces and electrostatic interactions. The notable role of -OH and $-NH_2$ groups from DOX in promoting adsorption suggests avenues for enhancing binding affinity through functionalization strategies (Zhang and Cai 2017).

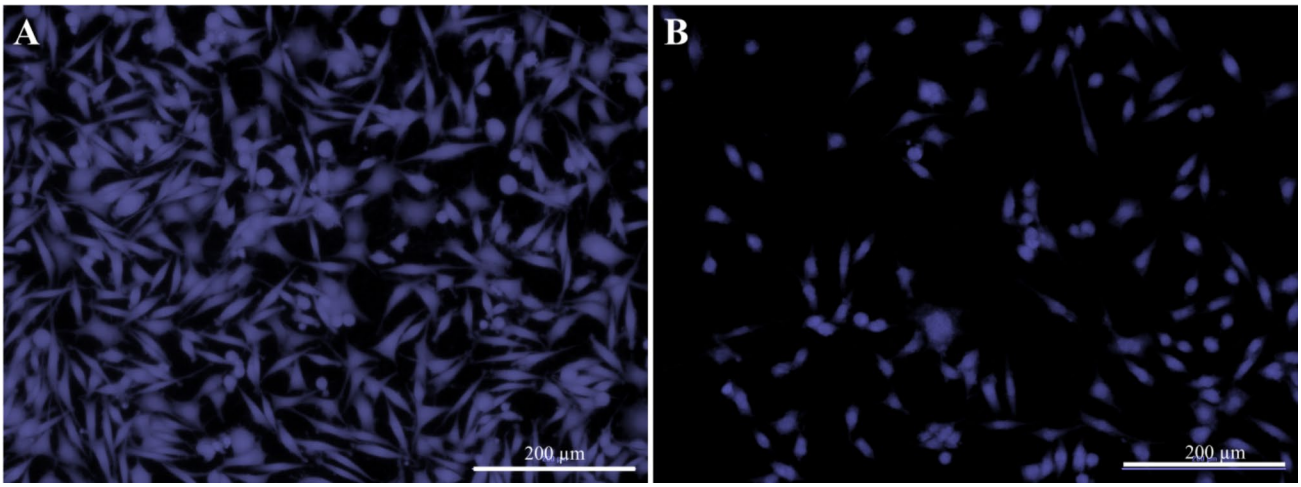


**Fig. 12** The transwell cell migration and invasion results. **A** Pure MXenes and **B** DOX@MXenes

### Stability of composite structures

The subsequent assembly of PVA-B onto the DOX/$Ti_3AlC_2$ structure was supported by Monte Carlo simulations, yielding adsorption energy of − 79.695 kJ/mol. This finding indicates stable composite formation, essential for ensuring sustained drug delivery. The resulting structural changes evident in the distortion of the DOX conformation and alterations in the MXene's surface morphology imply that these interactions can significantly influence the system's overall properties, potentially improving drug release profiles and targeting capabilities (Murali et al. 2021; Lin et al. 2021).

### In vitro drug release and cytotoxicity

The in vitro release studies conducted at two physiological pH levels (pH 5 and pH 7.4) demonstrated a noteworthy pH-dependent pattern, showcasing a burst release in acidic conditions (87.2% compared to 52.7% at neutral pH over 60 h). These findings align with earlier studies suggesting that acidic environments facilitate the hydrolysis of bond structures, thereby speeding up drug release. This phenomenon is especially beneficial for targeting tumor microenvironments, which are usually more acidic than normal tissues. Regarding cytotoxicity, the MTT assay results confirm the enhanced anti-cancer effectiveness of the DOX@MXene formulation. While pure MXene exhibited minimal cytotoxic effects, the conjugated system demonstrated significant dose-dependent toxicity, indicating that the combination of DOX with MXene not only augments therapeutic effects but also maintains a safety profile for the carrier material (Lin et al. 2021).

The apoptosis analysis using acridine orange/ethidium bromide staining offered additional confirmation of the anticancer mechanism, revealing a significant increase in apoptosis among treated cancer cells. This indicates that the conjugated formulation triggers oxidative stress pathways that result in cell death, supporting our hypothesis that this delivery system can successfully activate intrinsic apoptotic pathways (Porwal 2023).

### Anti-metastatic properties

The exploration of the anti-metastatic capabilities of nanoformulation through transwell migration assays highlights a significant reduction in invasive characteristics of cancer cells. The superior performance of DOX@MXenes compared to pure MXenes not only reinforces the therapeutic potential of this system but also underscores the importance of selecting appropriate drug delivery platforms that can effectively mitigate cancer cell dissemination (Liu et al. 2021).

This study highlights a remarkable improvement in drug delivery efficiency compared to earlier MXene systems, featuring better release profiles and targeted delivery methods. Additionally, the current formulation boasts enhanced biocompatibility, leading to lower cytotoxicity levels than those found in prior studies. Furthermore, it demonstrates greater stability under physiological conditions, tackling a common limitation noted in similar research.

However, despite these promising results, the scalability of this system for commercial use is still uncertain, echoing concerns raised in related studies. Also, when compared to some advanced nanocarrier systems, this MXene approach has a more limited target range for specific diseases, which could restrict its versatility. Overall, while significant progress has been made, it will be essential to address these remaining challenges for future therapeutic applications.

## Conclusions and future outlook

In this study, the research has exhibited the synthesis of DOX-conjugated MXenes as an efficient anti for treatment for lung cancer. The simulation studies (DFT-D and MD) based on Monte-Carlo simulation studies were conducted to assess the interactions. The energy minimization process was performed by using $DMol^3$ based on the DFT-D method. Then, $Ti_3AlC_2$ (104) surface with dimensions of $3.07 \times 3.07 \times 18.62$ $Å^3$ was prepared to load DOX and PVA-B compounds. Monte Carlo simulation was used to adsorb DOX over $Ti_3AlC_2$ (104) and PVA-B molecules on the DOX/ $Ti_3AlC_2$ (104). The thermodynamic parameter (Eads) revealed that the adsorption process is both spontaneous and endothermic, as indicated by the negative values. Biological evaluations demonstrated that the nanoformulation displayed pH-dependent drug release. Additionally, the synthesized nanoformulation exhibited dose-dependent cytotoxic effects on cells. These findings could support the development of a drug delivery system aimed at targeting the intrinsic apoptotic pathway. Thus, the synthesis and characterization of DOX-conjugated MXenes represent an exciting step forward in targeted lung cancer treatment. By integrating computational studies with experimental validations, we have gained a thorough understanding of the underlying interactions and mechanisms of action. The pH-dependent release profiles, improved cytotoxic effects, and pro-apoptotic properties of DOX@MXenes indicate its promise as an effective therapeutic system for cancer. Looking ahead, it is crucial to conduct additional studies to investigate the in vivo effectiveness of this formulation, along with thorough evaluations of its biocompatibility and pharmacokinetics.

Moreover, examining different MXene compositions and surface modifications could improve drug delivery potential, maximizing the therapeutic index of chemotherapeutics for lung cancer treatment. These insights open up new avenues for innovative strategies to address this challenging disease.

**Acknowledgements** The authors extend their appreciation to the Deanship of Research and Graduate Studies at King Khalid University for funding this work through a Large Research Project under grant number RGP2/460/45.

**Authors contributions** Conceptualization, Shan Fang, Yuan Li, Wenjuan Wu, Kun He, Nagaraj Patil; methodology, Shan Fang, Yuan Li, Wenjuan Wu, Kun He, Nagaraj Patil; formal analysis, Shan Fang, Yuan Li, Wenjuan Wu, Kun He, Nagaraj Patil; investigation, Shan Fang, Yuan Li, Wenjuan Wu, Kun He, Nagaraj Patil; writing—original draft preparation, Shan Fang, Yuan Li, Wenjuan Wu, Kun He, Nagaraj Patil; writing—review and editing, Shubham Sharma, Karthikeyan A, Dhirendra Nath Thatoi, Azath Mubarakali; supervision, Karthikeyan A, Dhirendra Nath Thatoi, Azath Mubarakali; project administration, Karthikeyan A, Dhirendra Nath Thatoi, Azath Mubarakali; funding acquisition, Karthikeyan A, Dhirendra Nath Thatoi, Azath Mubarakali. All authors have read and agreed to the published version of the manuscript. The authors declare that all data were generated in-house and that no paper mill was used.

**Funding** The authors extend their appreciation to the Deanship of Research and Graduate Studies at King Khalid University for funding this work through a Large Research Project under grant number RGP2/460/45.

**Data availability** All the characterizations, analysis, and testing-related work and testing's have solely been the responsibility of Kun He, and Shan Fang. Additionally, the raw data can be obtained on request from the corresponding authors, Kun He, and Shan Fang.

## Declarations

**Consent to participate** Not applicable.

**Consent for publication** All authors have read and approved this manuscript.

**Conflict of interest** The authors declare no competing interests.

## References

김유진 et al (2024) Enhanced flexibility, performance and oxidation stability of micro-supercapacitors fabricated by direct-ink-writing of MXene and PEDOT. 한국고분자학회 학술대회 연구논문 초록집 49(1):130–130

Ahlawat J et al (2020) Nanoparticles in biomedical applications. Green Nanoparticles: Synthesis and Biomedical Applications 227–250. https://doi.org/10.1007/978-3-030-39246-8_11

Aryal S et al (2009) Doxorubicin conjugated gold nanoparticles as water-soluble and pH-responsive anticancer drug nanocarriers. J Mater Chem 19(42):7879–7884

Balakrishnan N et al (2022) Effect of N-benzyl group in indole scaffold of thiosemicarbazones on the biological activity of their Pd (II) complexes: DFT, biomolecular interactions, in silico docking, ADME and cytotoxicity studies. Inorg Chim Acta 534:120805

Biswas AK, et al (2014) Nanotechnology based approaches in cancer therapeutics. Adv Nat Sci Nanosci Nanotechnol 5(4):043001

Ciruelos E, Jackisch C (2014) Evaluating the role of nab-paclitaxel (Abraxane) in women with aggressive metastatic breast cancer. Expert Rev Anticancer Ther 14(5):511–521

Darabdhara G et al (2019) Ag and Au nanoparticles/reduced graphene oxide composite materials: synthesis and application in diagnostics and therapeutics. Adv Coll Interface Sci 271:101991

Dorairaj DP et al (2023) Anti-proliferative potential of copper (I) acylthiourea complexes with triphenylphosphine against breast cancer cells. Appl Organomet Chem 37(6):e7087

Dorairaj DP et al (2023) Ru (II)-p-Cymene complexes of furoylthiourea ligands for anticancer applications against breast cancer cells. Inorg Chem 62(30):11761–11774

Ganjali Koli M, Eshaghi Malekshah R, Hajiabadi H (2023) Insights from molecular dynamics and DFT calculations into the interaction of 1, 4-benzodiazepines with 2-hydroxypropyl-βCD in a theoretical study. Sci Rep 13(1):9866

Geethakumari D et al (2022) Folate functionalized chitosan nanoparticles as targeted delivery systems for improved anticancer efficiency of cytarabine in MCF-7 human breast cancer cell lines. Int J Biol Macromol 199:150–161

Gholivand K et al (2023) New phosphoramides containing 2-amino-1, 4-naphthaquinone moiety as anticancer and antibacterial agents: experimental and theoretical evaluations. Process Biochem 132:97–109

Haounati R et al (2023a) Z-Scheme g-C3N4/Fe3O4/Ag3PO4@ Sep magnetic nanocomposites as heterojunction photocatalysts for green malachite degradation and dynamic molecular studies. Colloids Surf, A 671:131509

Haounati R et al (2023b) Exploring ZnO/montmorillonite photocatalysts for the removal of hazardous RhB Dye: a combined study using molecular dynamics simulations and experiments. Mater Today Commun 35:105915

Ho BN, Pfeffer CM, Singh AT (2017) Update on nanotechnology-based drug delivery systems in cancer treatment. Anticancer Res 37(11):5975–5981

Ighnih H et al (2023) Sunlight driven photocatalytic degradation of RhB dye using composite of bismuth oxy-bromide kaolinite BiOBr@ Kaol: experimental and molecular dynamic simulation studies. J Photochem Photobiol A Chem 445:115071

Ighnih H et al (2023) Photocatalytic degradation of RhB dye using hybrid nanocomposite BiOCl@ Kaol under sunlight irradiation. J Water Process Eng 54:103925

Iravani S, Varma RS (2021) MXenes and MXene-based materials for tissue engineering and regenerative medicine: Recent advances. Mater Adv 2(9):2906–2917

Jamalipour Soufi G et al (2022) MXenes and MXene-based materials with cancer diagnostic applications: challenges and opportunities. Comments Inorg Chem 42(3):174–207

Jiang M et al (2024) Evolution of surface chemistry in two-dimensional MXenes: from mixed to tunable uniform terminations. Angew Chem 136(37):e202409480

Kawasaki ES, Player A (2005) Nanotechnology, nanomedicine, and the development of new, effective therapies for cancer. Nanomed: Nanotechnol Biol Med 1(2):101–109

Khazaei M et al (2017) Electronic properties and applications of MXenes: a theoretical review. J Mater Chem C 5(10):2488–2503

Kratzer TB et al (2024) Lung cancer statistics, 2023. Cancer 130(8):1330–1348

Lele N et al (2023) Construction of a multifunctional MXene@ β-cyclodextrin nanocomposite with photocatalytic properties. Emergent Mater 6(2):605–626

Lin X et al (2021) Fascinating MXene nanomaterials: emerging opportunities in the biomedical field. Biomater Sci 9(16):5437–5471
Liu Z et al (2021) Folic acid-targeted MXene nanoparticles for doxorubicin loaded drug delivery. Aust J Chem 74(12):847–855
Maleki A et al (2022) Biomedical applications of MXene-integrated composites: regenerative medicine, infection therapy, cancer Treatment, and biosensing. Adv Func Mater 32(34):2203430
Miao B et al (2024) Impact of various 2D MXene surface terminating groups in energy conversion. Renew Sustain Energy Rev 199:114506
Miele E, Spinelli GP, Miele E, Tomao F, Tomao S (2009) Albumin-bound formulation of paclitaxel (Abraxane ABI-007) in the treatment of breast cancer. Int J Nanomedicine. 4:99–105. https://doi.org/10.2147/ijn.s3061
Mozafari M, Soroush M (2021) Surface functionalization of MXenes. Mater Adv 2(22):7277–7307
Murali A et al (2021) Emerging 2D nanomaterials for biomedical applications. Mater Today 50:276–302
Oliveira JdS, Guidelli EJ (2021) Multitherapeutic nanoplatform based on scintillating anthracene, silver@ anthracene, and gold@ anthracene nanoparticles for combined radiation and photodynamic cancer therapies. Mater Sci Eng C 126:112122
Pao W, Girard N (2011) New driver mutations in non-small-cell lung cancer. Lancet Oncol 12(2):175–180
Paramasivam G et al (2024) Recent advances in the medical applications of two-dimensional MXene nanosheets. Nanomedicine 19(30):2633–2654
Parhi P, Mohanty C, Sahoo SK (2012) Nanotechnology-based combinational drug delivery: an emerging approach for cancer therapy. Drug Discov Today 17(17–18):1044–1052
Porwal R (2023) Development of lipid nanoparticles based drug delivery systems targeting oxidative stress for disease prevention and therapy-preeclampsia to acute lung injury. The University of Nebraska-Lincoln
Ramalingam V et al (2018) Target delivery of doxorubicin tethered with PVP stabilized gold nanoparticles for effective treatment of lung cancer. Sci Rep 8(1):3815
Rasid ZM, et al (2017) Low cost synthesis method of two-dimensional titanium carbide MXene. In: IOP Conference Series: Materials Science and Engineering. IOP Publishing
Rizwan K, Khan A, Asiri AMA (n.d.) Handbook of functionalized nanostructured MXenes. Smart Nanomaterials Technology. https://doi.org/10.1007/978-981-99-2038-9
Ruan S et al (2015) Tumor microenvironment sensitive doxorubicin delivery and release to glioma using angiopep-2 decorated gold nanoparticles. Biomaterials 37:425–435
Siegel RL et al (2023) (2023) Cancer statistics. CA CancerJ Clin 73(1):17–48
Sun S et al (2021) Rapid synthesis of polyimidazole functionalized MXene via microwave-irradiation assisted multi-component reaction and its iodine adsorption performance. J Hazard Mater 420:126580
Urso M et al (2022) Trapping and detecting nanoplastics by MXene-derived oxide microrobots. Nat Commun 13(1):3573
Yamamoto H, Toyooka S, Mitsudomi T (2009) Impact of EGFR mutation analysis in non-small cell lung cancer. Lung Cancer 63(3):315–321
Yao N et al (2022) Synergistic adsorption and oxidative degradation of polyvinyl alcohol by acidified OMS-2: Catalytic mechanism, degradation pathway and toxicity evaluation. Sep Purif Technol 302:122047
Zarogoulidis P et al (2013) Intensive care unit and lung cancer: when should we intubate? J Thorac Dis 5(Suppl 4):S407
Zhang J, Cai K (2017) Integration of polymers in the pore space of mesoporous nanocarriers for drug delivery. J Mater Chem B 5(45):8891–8903

## Authors and Affiliations

**Shan Fang[1] · Yuan Li[2] · Wenjuan Wu[3] · Kun He[4] · Nagaraj Patil[5] · Shubham Sharma[6,7,8] · Karthikeyan A.[9] · Dhirendra Nath Thatoi[10] · Azath Mubarakali[11]**

✉ Kun He
hekun060708@hotmail.com

Shan Fang
fangshan0600@outlook.com

Yuan Li
liyuan19840518@163.com

Wenjuan Wu
13833305221@163.com

Shubham Sharma
shubham543sharma@gmail.com;
shubhamsharmacsirclri@gmail.com

1 Department of Respiratory and Critical Care Medicine, Union Hospital, Tongji Medical College, Huazhong University of Science and Technology, No. 1277, Jiefang Road, Wuhan City, Hubei Province 430022, China

2 Department of Respiratory Medicine, Shanxi Province Cancer Hospital, Shanxi Hospital Affiliated to Cancer Hospital, Chinese Academy of Medical Sciences, Cancer Hospital Affiliated to Shanxi Medical University, Taiyuan 030013, China

3 Department of Medical Oncology, The First Affiliated Hospital of Hebei North University, No.36, Changqing District, Zhangjiakou 075000, China

4 Department of Emergency, Shanxi Bethune Hospital, Shanxi Academy of Medical Sciences, Tongji Shanxi Hospital, Third Hospital of Shanxi Medical University, Taiyuan 030032, China

5 Department of Mechanical Engineering, School of Engineering and Technology, JAIN (Deemed to Be University), Bangalore, Karnataka, India

6 Department of Technical Sciences, Western Caspian University, Baku, Azerbaijan

7 Centre for Research Impact and Outcome, Chitkara University Institute of Engineering and Technology, Chitkara University, Rajpura 140401, Punjab, India

8 Jadara University Research Center, Jadara University, Irbid, Jordan

9 Department of Mechanical Engineering, Sathyabama Institute of Science and Technology, Chennai, Tamil Nadu, India

10 Department of Mechanical Engineering, Siksha 'O' Anusandhan (Deemed to Be University), Bhubaneswar, Odisha 751030, India

11 Department of Informatics and Computer Systems, College of Computer Science, King Khalid University, Abha, Kingdom of Saudi Arabia